Journal of Solid State Chemistry 184 (2011) 2834–2839

Contents lists available at SciVerse ScienceDirect

Journal of Solid State Chemistry

journal homepage: www.elsevier.com/locate/jssc

Phase stability of some actinides with brannerite structure at high pressures

F.X. Zhang [a], M. Lang [a], Zhenxian Liu [b], R.C. Ewing [a,*]

[a] Department of Geological Sciences, University of Michigan, Ann Arbor, MI 48109, United States
[b] Geophysical Laboratory, Carnegie Institute of Washington, DC 200015, United States

ARTICLE INFO

Article history:
Received 13 April 2011
Received in revised form
1 August 2011
Accepted 15 August 2011
Available online 24 August 2011

Keywords:
Brannerite
Actinide
High pressure
Amorphization

ABSTRACT

Structure behavior of actinide brannerites $ThTi_2O_6$, $Y_{0.5}U_{0.5}Ti_{1.5}Nb_{0.5}O_6$ and their analog oxide $CeTi_2O_6$ was studied at high pressure by using *in situ* x-ray diffraction, Raman scattering and infra-red absorption techniques, respectively. Brannerite structure was found to be not stable and started to become amorphous at pressures above 20 GPa. Some minor crystalline phase(s) due to phase decomposition was observed in all the three samples during pressurization. In addition, the observed bulk modulus indicated that the actinide-bearing brannerites are more compressible than their analog compound $CeTi_2O_6$, which may be related to the asymmetric 5*f* electron orbits of actinide elements.

1. Introduction

Brannerite is a common accessory phase found in uranium ore deposition and is one of the principle uranium minerals [1,2]. Since it is a host for uranium metal in nature and very stable in open environments, brannerite, such as UTi_2O_6 is a minor phase in pyrochlore–zirconolite ceramics, which is designed for the immobilization of actinide-rich and plutonium-bearing nuclear waste [3,4]. Brannerite crystallizes in monoclinic symmetry (space group *C*2/*m*) and the TiO_6 octahedra form corner and edge-sharing layers and the large cations reside in the voids between Ti–O layers (Fig. 1). Since brannerite is a layered structure and there are big channels between the layers, which are suitable for the transportation of large ions, some transition metal oxides with brannerite-type structure, such as $LiWVO_6$, MnV_2O_6 and ZnV_2O_6, etc. have been proposed as electrode materials for lithium ion rechargeable batteries [5–7]. Cerium is thought to be an analog or model for uranium and plutonium containing compounds because of its high molecular mass and similar electronic structure to actinide metals. Thermal properties and structural response to ion irradiation for Ce- and Ac-rich brannerite have been studied before [8–11].

The study of brannerite and other actinides at extreme conditions is not only important to basic science but also to the application of these materials in nuclear engineering. Natural brannerite mineral is nearly always x-ray amorphous because of self-radiation damage from α-decay of U, Th and their daughter isotopes. During ion irradiation, brannerite oxides are easy to be amorphized due to the energy deposition from implanted ions [8]. There is no complete phase diagram for Ac–Ti–O systems, and it is believed that brannerite is stable at least to its synthetic temperature (above 1000 °C). Pressure is another external parameter and pressure-induced structural changes are well known. To radioactive materials, it is not clear now whether pressure will affect their radiation properties, however, pressure can do change the bonding status and crystal structures of actinide-bearing materials [12–14]. Previous studies revealed that there are quite a lot of similarities during the processes of ion irradiation and pressurization to many compounds, especially in pyrochlore oxides [15–18]. However, the structure response of brannerite oxides at high pressures was not reported before. In this study, the structural behavior of synthetic brannerite oxides $CeTi_2O_6$, $ThTi_2O_6$ and $(Y_{0.5}U_{0.5})(Ti_{0.75}Nb_{0.25})_2O_6$ at pressures up to 50 GPa have been investigated by *in situ* x-ray diffraction (XRD), Raman scattering and far infra-red (FIR) absorption measurements.

2. Experimental details

All the brannerites were synthetic powders, which were made with solid state reaction method and the details of synthesis process can be found elsewhere [10]. Small amount of impurities can be found in the U-brannerite by XRD measurement. Pressure was generated with diamond anvil cell techniques. Stainless steel gasket was indented to ~40 μm and a hole with less than 120 μm in diameter was drilled in the center, which serves as pressure chamber. Pressure was calibrated with standard ruby fluorescence method. Methanol/ethanol mixture (4/1 volume ratio) was used as pressure

* Corresponding author.
E-mail address: rodewing@umich.edu (R.C. Ewing).

0022-4596/$ - see front matter © 2011 Elsevier Inc. All rights reserved.
doi:10.1016/j.jssc.2011.08.022

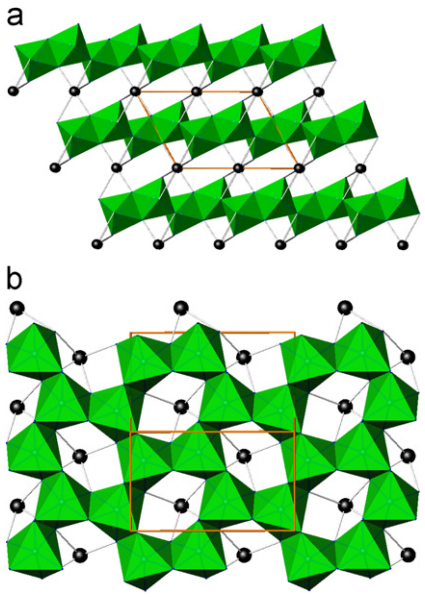

Fig. 1. Schematic crystal structure of brannerite: (a) view along [010] direction and (b) single layer of brannerite structure with edge sharing Ti–O octahedra and the large cations reside in the voids.

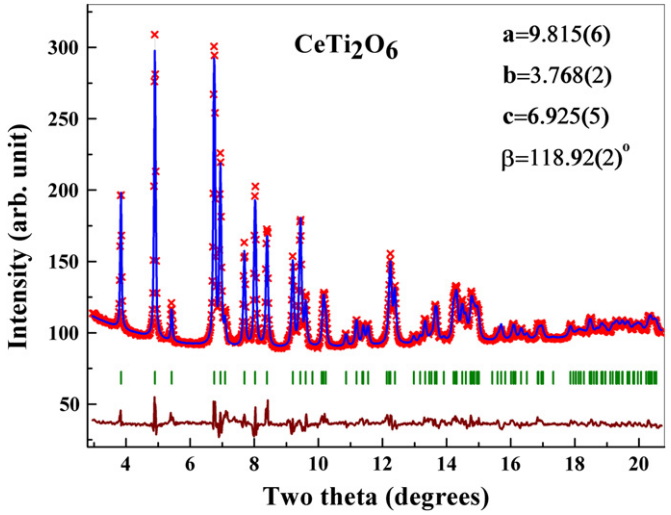

Fig. 2. Rietveld refinement of room condition XRD pattern of $CeTi_2O_6$ with brannerite structure model.

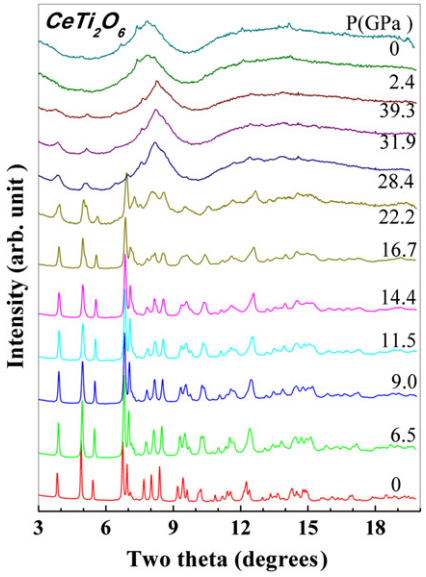

Fig. 3. Selected XRD patterns of $CeTi_2O_6$ at high pressures. Brannerite-type $CeTi_2O_6$ is stable up to 14.4 GPa and it starts to amorphize at pressure above 22 GPa. Phase decomposition was found during amorphization.

medium for XRD and Raman measurements, which can keep good hydrostatic conditions up to ~10 GPa. XRD experiments were performed at x17C station of National Synchrotron Light Source (NSLS), Brookhaven National Laboratory, and B2 station of Cornell High Energy Synchrotron Source (CHESS), Cornell University. The wavelength of x-ray beam is 0.4066 Å at NSLS and 0.486 Å at CHESS. Debye rings were recorded with a Mar CCD detector in NSLS and Mar 345 image plate detector in CHESS, respectively. The two-dimensional patterns were integrated from the collected images through software Fit 2d [19]. Lattice parameters and atomic coordinates were derived from Rietveld refinement of the XRD patterns with program Fullprof [20]. Raman spectrum was measured with a Spex-1250 Raman spectrometer attached with a liquid nitrogen cooled CCD detector (Symphony). Green light (514.53 nm) from an Ar laser is used as the activation light source. The far IR absorption spectra at high pressure were measured at U2A station of NSLS with a pair of selected ultralow fluorescence type-II diamond anvils in a quasihydrostatic condition with pressure medium of vasaline.

3. Results and discussion

3.1. XRD experiments

The XRD pattern of $CeTi_2O_6$ at room conditions can be well refined with the brannerite structure model (Fig. 2) and the refined lattice parameters are $a=9.815(6)$ Å, $b=3.768(2)$ Å, $c=6.925(5)$ Å, and $\beta=118.92(2)^\circ$, which are consistent with those in the literature [21]. The *in situ* XRD patterns of $CeTi_2O_6$ at high pressure were collected at NSLS and Fig. 3 shows the selected XRD patterns of $CeTi_2O_6$ at different pressures. The brannerite structure is stable up to 14.4 GPa from the observed XRD patterns. Starting from 16.7 GPa, the first two diffraction peaks are obviously broadened and became doublet at pressure of 22.2 GPa, which suggests pressure-induced phase transition(s) or phase decomposition in this oxide. With further increase of pressure, a broad diffused scattering at two theta around 8° starts to appear in the XRD pattern at 22.2 GPa and this is due to the formation of amorphous. The pressure-induced crystalline to crystalline phase transition (or decomposition) and amorphization in $CeTi_2O_6$ may occur simultaneously and the minor crystalline phases remain after the brannerite was fully amorphized. No diffractions from brannerite can be observed in the XRD patterns from 31.9 GPa, however, some diffraction peaks from the transformed crystalline phases are still observable at high pressures and during the process of pressure release. The pressure-induced amorphization is an irreversible process and the amorphous phase is quenchable. In order to identify the crystalline phases during amorphization, the *d*-values of the diffraction peaks in the quenched sample were compared with all the known structures in Ce–Ti–O ternary system. We found that the crystalline diffractions in the quenched samples mainly belong to Ce_2TiO_5 and some peaks may be contributed to TiO_2 (anatase). Table 1 lists the observed *d*-values and the main diffraction peaks from Ce_2TiO_5 and anatase TiO_2. The ternary compound Ce_2TiO_5 crystallizes in an orthorhombic unit cell, which is isostructural with La_2TiO_5 [22,23]. The cations in La_2TiO_5 compound have 7 and 5 coordinates with oxygen, respectively and it is a stable phase to most light rare earth element titanates at ambient conditions. The observed *d*-values have larger difference from the diffraction peaks of anatase, and this may be due to the

Table 1
The observed *d*-values of crystalline diffraction peaks in the quenched sample of $CeTi_2O_6$ and comparison with the main diffractions of Ce_2TiO_5 (PDF-49-1606) and TiO_2 (anatase, PDF-21-1272).

No.	Observed peaks		Ce_2TiO_5			TiO_2 (anatase)		
	2θ (deg.)	d (Å)	(hkl)	I/I_0	d (Å)	(hkl)	I/I_0	d (Å)
1	4.86	4.80	(201)	6	4.91			
2	6.67	3.49				(101)	100	3.52
3	7.39	3.15	(210)	100	3.17			
4	7.52	3.10	(203)	73	3.11			
5	8.52	2.74	(013)	38	2.72			
6	12.06	1.94	(020)	34	1.95			
7	12.13	1.92	(413)	73	1.92	(200)	65	1.89
8	14.16	1.65				(105)	41	1.70
						(211)	42	1.67

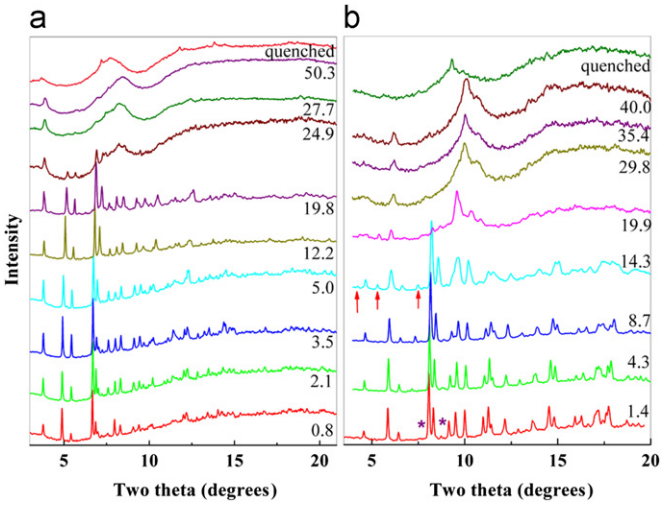

Fig. 4. Selected XRD patterns of (a) $ThTi_2O_6$ and (b) $Y_{0.5}U_{0.5}Ti_{1.5}Nb_{0.5}O_6$ at various pressures. Pressure-induced amorphization and partial decomposition are observed in both samples.

nonstoichiometry during decomposition. From the observed XRD patterns, we can conclude that small amount of brannerite-type $CeTi_2O_6$ decomposed into the orthorhombic Ce_2TiO_5 and anatase at high pressures, and decomposition may take place simultaneously with amorphization.

The selected XRD patterns of $ThTi_2O_6$ and $(U_{0.5}Y_{0.5})(Ti_{1.5}Nb_{0.5})O_6$ are shown in Fig. 4a and b, respectively. The XRD patterns of $(U_{0.5}Y_{0.5})(Ti_{1.5}Nb_{0.5})O_6$ were collected at CHESS with x-ray wavelength of 0.486 Å. The phase behavior of $ThTi_2O_6$ is very close to the case of $CeTi_2O_6$. The brannerite structure is stable till to 19.8 GPa and an amorphous phase was observed at higher pressures. The amorphization process completed at 27.7 GPa, however, some weak diffraction peaks are still observable till to 50.3 GPa. This is due to the formation of small amount of crystalline phases during pressurization, and the similar character of the crystalline diffraction peaks suggests that the decomposed crystalline phases are probably the orthorhombic Th_2TiO_5 and anatase. There is no structural report about the compound Th_2TiO_5, and the 3–4 observed diffraction peaks is not enough to derive reliable lattice parameters. The XRD patterns of $(U_{0.5}Y_{0.5})(Ti_{1.5}Nb_{0.5})O_6$ indicated that there is a minor impurity phase in this sample. Pressure-induced amorphization was confirmed to start at 19.9 GPa. To the XRD pattern at 14.3 GPa, several new diffraction peaks can be observed, and it is due to the pressure-induced phase decomposition of brannerite. The crystalline diffraction peak at two theta of 6° is still observable at 40 GPa. It is not from the brannerite structure but from the new crystalline phase, because the strongest diffraction maximum of brannerite structure was completely disappeared at pressures of 29.8 GPa. The XRD patterns of U-bearing brannerite are more complicated than the other two brannerite compounds because of its more complex chemical composition.

The *in situ* XRD patterns of the three brannerite oxides show similar structure behavior at high pressures and an irreversible amorphization process was observed. Small amount of brannerites decomposed into compounds of orthorhombic A_2TiO_5 (A=Ce, Th, U/Y) phase and anatase, and the decomposition process took place simultaneously with amorphization. The decomposition in U-bearing brannerite is more complicated because of it complex chemical composition. The pressure medium (ethanol/methanol mixture) used in our experiments can keep good hydrostatic condition till to 10 GPa, and the pressure is quasi-hydrostatic condition at higher pressures. Previous experiments indicated that similar structural changes can always be found in both hydrostatic and quasi-hydrostatic conditions, and stress induced by non-hydrostatic pressure can only make the process easier and lower the critical pressure. So we believe that pressure-induced phase decomposition and amorphization in brannerite is intrinsic. Pressure-induced amorphization and irradiation-induced amorphization in brannerite have obvious difference, and no phase decomposition was found in the letter [8].

The lattice parameters of brannerite at high pressures were derived from the Rietveld refinement of the observed XRD patterns. Fig. 5 shows the results of the XRD patterns of $ThTi_2O_6$ and $(U_{0.5}Y_{0.5})(Ti_{1.5}Nb_{0.5})O_6$ refined with brannerite structure at 5.7 GPa and 4.3 GPa, respectively. The pressure dependence of the unit cell volume of the three brannerite oxides was shown in Fig. 6 till to pressures around 20 GPa. Bulk modulus of brannerites through fitting

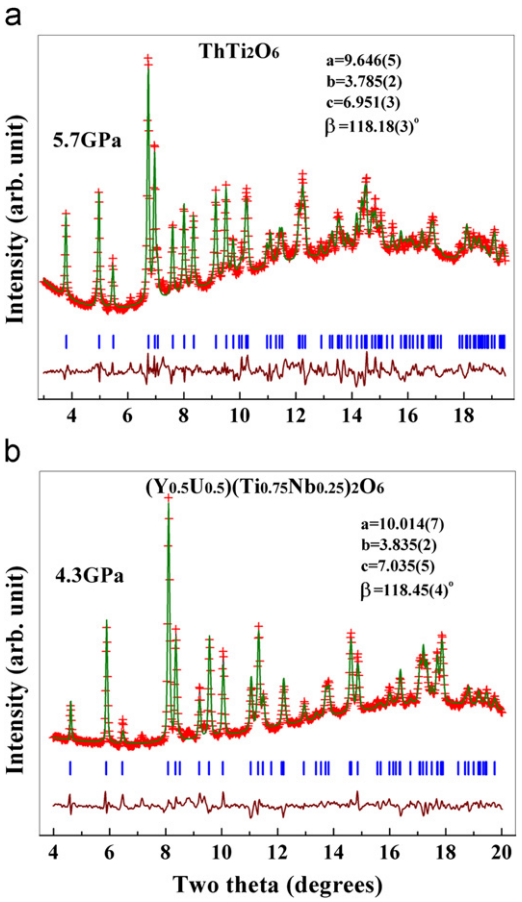

Fig. 5. Observed and calculated XRD patterns of (a) $ThTi_2O_6$ at 5.7 GPa and (b) $Y_{0.5}U_{0.5}Ti_{1.5}Nb_{0.5}O_6$ at 4.3 GPa from Rietveld refinement with brannerite structure model.

of the *P–V* curves with Murnaghan equation of state (the zero pressure derivatives are all fixed at 4) is listed in Table 2. The bulk modulus $CeTi_2O_6$ is 166 GPa and Th- and U-brannerites is about 38% and 15% smaller than that of $CeTi_2O_6$. Comparing to Th-brannerite, the difference of bulk modulus between U-brannerite and Ce-brannerite is not so significant. This is mainly due to the doping of Y^{3+} on the U-site in the brannerite structure. It is expected that smaller bulk modulus similar to that of $ThTi_2O_6$ will be observable in the pure U-brannerite though we have no brannerite UTi_2O_6. Recent theoretical investigation has revealed that the 5*f* electrons of Pu have more asymmetric orbits than Ce [24]. It is reasonable to believe that the larger compressibility of actinide-bearing brannerite is caused by the 5*f* electrons in the compounds.

3.2. Raman spectra of $ThTi_2O_6$

The Ce- and U-contained brannerites are in dark color and $ThTi_2O_6$ is transparent to visible light. Raman measurement found that only $ThTi_2O_6$ brannerite has good Raman signal. The Raman spectra of $ThTi_2O_6$ at various pressures are shown in Fig. 7. At pressures higher than 23.5 GPa, there is only one broad band between 700 and 850 cm^{-1} observable in the profile. That is due to amorphization and the pressure-induced amorphization is irreversible during unloading pressure, which is consistent with XRD measurements. However, it is interesting that at pressure of 4.6 GPa, we observed obviously disappearance of brannerite modes and appearing of new Raman modes in $ThTi_2O_6$. The first mode centered at ~150 cm^{-1} disappeared gradually and a new band with frequency close to that became stronger and stronger with the increase of pressure. At least, another two or three Raman modes start to appear after 4.6 GPa and the strongest band at frequency around 620 cm^{-1} starts to split after 4.6 GPa.

Group theory suggests that brannerite has totally 12 Raman active modes in the Brillouin center: $\Gamma_{Raman}=4(2A_g+B_g)$. In our measurements, there are totally 10 modes clearly observed in the Raman spectrum of $ThTi_2O_6$ at room conditions. It is impossible to index these Raman modes from the powder measurement. Based on previous Raman experiments on transition metal vanadate MV_2O_6 (M transition metal) with brannerite structure [25], two Raman active modes, which centered at 195 and 760 cm^{-1}, are contributed to the O–Ti–O stretching. They changed continuously until disappeared after amorphization.

The Raman spectra of $ThTi_2O_6$ at high pressure became quite complicated. The pressure dependence of the frequencies of the observed Raman active modes is plotted in Fig. 8. There are two obvious pressure-induced structural changes in $ThTi_2O_6$. One is at 4.6 GPa and the second one is close to 14 GPa. The first structural change at 4.6 GPa was not found from the XRD measurement. The pressure dependence of lattice parameters of $ThTi_2O_6$ is shown in Fig. 9 and there is no obvious discontinued change at pressure around 4.6 GPa. However, we found that the new Raman modes appeared at 4.6 GPa in $ThTi_2O_6$ are quite close to the vibrational modes of anatase (TiO_2) [26]. So the structural change at 4.6 GPa may be due to the partial decomposition of brannerite. Measurement of anatase indicated that the Raman modes of anatase are very strong, even to very small amount of powders. Due to the weak x-ray scattering ability of TiO_2, small amount of TiO_2 may be not observable from XRD measurement. In fact, the two strongest diffraction peaks of anatase are nearly overlapped with the strong diffraction peaks of brannerite at 2θ of ~8° and ~12°. It is reasonable to believe that the structural change in $ThTi_2O_6$ at 4.6 GPa from Raman measurement is due to the decomposition of small amount of brannerite. The unit cell volume of brannerite has no obviously discontinuous change at this pressure. The pressure dependence of the beta angle of the unit cell seems to have a sudden decrease at lower pressures, which may be related to the phase decomposition process observed from Raman measurements. The structural change at 14 GPa is obviously related to pressure-induced amorphization of brannerite structure.

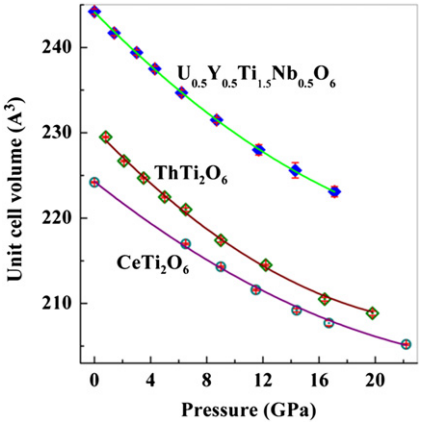

Fig. 6. *P–V* curves of brannerite-type oxides of $CeTi_2O_6$, $ThTi_2O_6$ and $Y_{0.5}U_{0.5}Ti_{1.5}Nb_{0.5}O_6$.

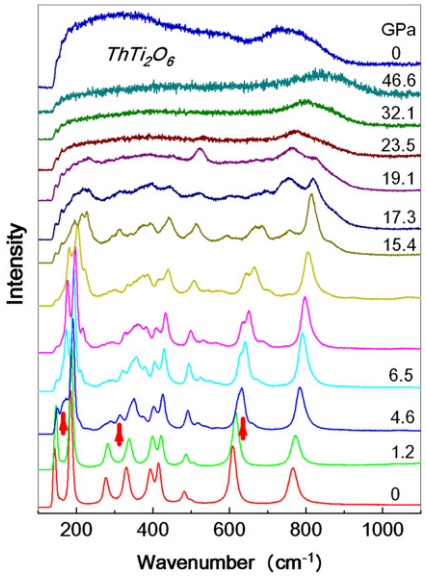

Fig. 7. Selected Raman spectra of $ThTi_2O_6$ at various pressures, the new Raman modes marked with arrows are due to the anatase-like phase from phase decomposition.

Table 2
Bulk modulus of brannerites $CeTi_2O_6$, $ThTi_2O_6$ and $Y_{0.5}U_{0.5}Ti_{1.5}Nb_{0.5}O_6$ derived from the fitting of *P–V* curves with Murnagham equation of state.

Bulk modulus	$CeTi_2O_6$	$ThTi_2O_6$	$Y_{0.5}U_{0.5}Ti_{1.5}Nb_{0.5}O_6$
B (GPa)	161(19), B'_0=9.5(2.9)	99.6(10), B'_0=11.3(1.9)	137.6(5.5), B'_0=6.7(0.9)
B (GPa), B'_0=4	199(7.7)	151.2(6.3)	153.2(2.6)

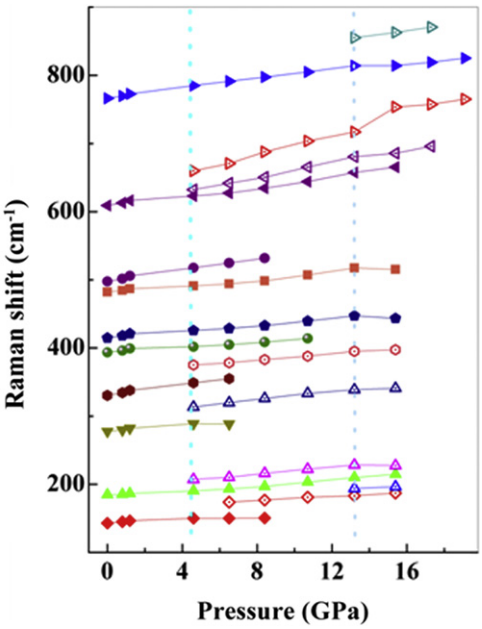

Fig. 8. Pressure dependence of the frequency of the Raman modes of $ThTi_2O_6$. The addition of Raman modes at 4.6 GPa and at higher pressures are due to phase decomposition.

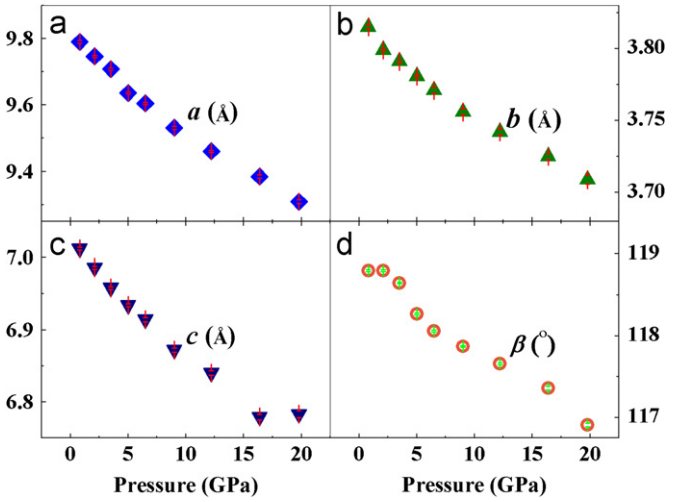

Fig. 9. Pressure dependence of lattice parameters of $ThTi_2O_6$. The continuous change of lattice parameters does not suggest any phase transition at lower pressures.

3.3. *Far IR absorption of $ThTi_2O_6$*

In order to check any structural changes with pressure, optical absorption was measured in the far infrared region ($<700\ cm^{-1}$) and the absorption profiles at various pressures are shown in Fig. 10. In brannerite structure, Ti and three oxygen atoms reside on 4*c* position and each one contributes one A_u mode and 2 B_u modes in IR. Actinide element on the 2*a* site also contributes one A_u and 2 B_u modes. In the far infrared region ($<700\ cm^{-1}$), 8–9 IR active modes were observed. At 27.9 GPa and above, there is only one broad band in the spectrum, which corresponds to the pressure-induced amorphization of brannerite. This is consistent with XRD and Raman measurements. Due to the broad width of the observed IR modes, it is difficult to get the pressure dependence of their frequencies, but the continuous change of vibrational modes with pressure do not suggest any phase transitions before amorphization. The far infrared profiles of $CeTi_2O_6$ at high pressure are very similar to those of $ThTi_2O_6$.

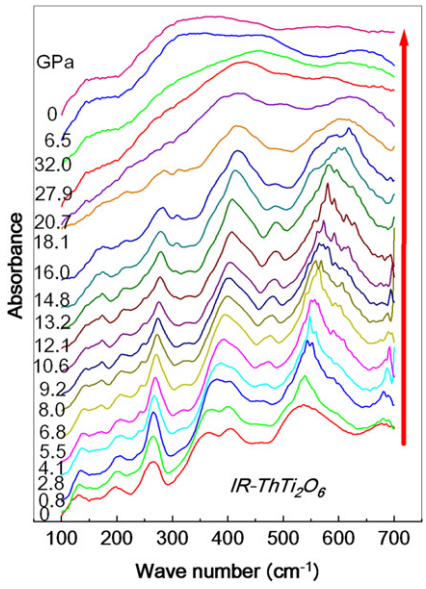

Fig. 10. Far infrared absorption spectra of $ThTi_2O_6$ at various pressures.

4. Summary

In the present work, structural changes of three compounds $CeTi_2O_6$, $ThTi_2O_6$ and $Y_{0.5}U_{0.5}Ti_{1.5}Nb_{0.5}O_6$ with brannerite-type structure were studied at pressures till to more than 40 GPa with *in situ* XRD, Raman scattering and infrared absorption methods. Experimental results indicate that brannerite-type structure is only stable at pressure below 20 GPa and became amorphous at higher pressures and the amorphization process is irreversible. Besides amorphous was found in the quenched samples, small amount of crystalline phases coexists during the whole process. This is caused by some minor phase decomposition accompanying amorphization during pressurization. The bulk modulus of actinide-bearing brannerites is smaller than that of their analog oxide ($CeTi_2O_6$) which is due to the asymmetric orbits of 5*f* electrons of actinide elements. Raman measurements also suggested a pressure-induced decomposition in $ThTi_2O_6$ may start before amorphization.

Acknowledgment

This work was supported as part of the Materials Science of Actinides, an Energy Frontier Research Center, funded by the Office of Basic Energy Sciences under Award number DE-SC0001089. The use of x-ray beam line at X17C and infrared at U2A station of NSLS was supported by NSF COMPRES EAR01-35554 and by US-DOE contract DE-AC02-10886. The use of Cornell High Energy Synchrotron Source was financially supported by NSF DMR-0936384 and NIH/NCRR RR-01646.

References

[1] D.F. Hewett, J. Stone, H. Levine, Am. Mineral. 42 (1957) 30–38.
[2] R. Ruh, A.D. Wadsley, Acta Crystallogr. 21 (1966) 974–978.
[3] N.P. Laverov, S.V. Yudintsev, T.S. Yudintseva, S.V. Stefanovsky, R.C. Ewing, J. Lian, S. Utsunomiya, L.M. Wang, Geol. Ore Deposits 45 (2003) 423–451.
[4] M. Collela, G.R. Lumpkin, Z. Zhang, E.C. Buck, K.L. Smith, Phys. Chem. Miner. 32 (2005) 52–64.
[5] Hk. Muller-Buschbaum, M. Kobel, J. Alloys Compd. 176 (1991) 39–46.
[6] K. Mocala, J. Ziolkowski, J. Solid State Chem. 69 (1987) 299–311.
[7] P.K. Davies, C.M. Kagan, Solid State Ionics 53–56 (1992) 546–552.
[8] J. Lian, L.M. Wang, G.R. Lumpkin, R.C. Ewing, Nucl. Instrum. Methods—Phys. Res. B 191 (2002) 565–570.

[9] K.B. Helean, A. Navrotsky, G.R. Lumpkin, M. Colella, J. Lian, R.C. Ewing, B. Ebbinghaus, J.G. Catalano, J. Nucl. Mater. 320 (2003) 231–244.
[10] G.R. Lumpkin, K.L. Smith, M.G. Blackford, J. Nucl. Mater. 289 (2001) 177–187.
[11] S.V. Yudintsev, S.V. Stefanovskii, O.I. Kir'yanova, J. Lian, R.C. Ewing, Atomic Energy 90 (2001) 487–494.
[12] F.X. Zhang, V. Pointeau, L.C. Shuller, D.M. Reaman, M. Lang, Zhenxian Liu, Jingzhu Hu, W.R. Panero, U. Becker, C. Poinssot, R.C. Ewing, Am. Mineral. 94 (2009) 916.
[13] M. Idiri, T. Le Bihan, S. Heathman, J. Rebizant, Phys. Rev. B 70 (2004) 014113.
[14] P.P. Bose, R. Mittal, S.L. Chaplot, Phys. Rev. B 79 (2009) 174301.
[15] F.X. Zhang, J.W. Wang, J. Lian, M.K. Lang, U. Becker, R.C. Ewing, Phys. Rev. Lett. 100 (2008) 045503.
[16] M. Lang, F.X. Zhang, J. Zhang, J. Wang, B. Schuster, C. Trautmann, R. Neumann, U. Becker, R.C. Ewing, Nat. Mater. 8 (2009) 793.
[17] F.X. Zhang, M. Lang, Z. Liu, R.C. Ewing, Phys. Rev. Lett. 105 (2010) 015503.
[18] F.X. Zhang, B. Manoun, S.K. Saxena, C.S. Zha, Appl. Phys. Lett. 86 (2005) 1811906.
[19] A.P. Hammersley, Fit 2d, ESRF, Grenoble, France, 1998.
[20] T. Roisnel, J. Rodriguez-Carvajal, in: Materials Science Forum, Proceedings of the Seventh European Powder Diffraction Conference (EPDIC7), 2000, 118 pp.
[21] M. Yoshida, N. Koyama, T. Ashizawa, Y. Sakata, H. Imamura, Jpn. J. Appl. Phys. 46 (2007) 977–979.
[22] F.X. Zhang, J.W. Wang, M. Lang, J.M. Zhang, R.C. Ewing, J. Solid State Chem. 183 (2010) 2636.
[23] A. Preuss, R. Gruehn, J. Solid State Chem. 110 (1994) 363.
[24] E.D.A. Ferriss, R.C. Ewing, U. Becker, Am. Mineral. 95 (2010) 229–241.
[25] E.J. Baran, C.J. Cabello, A.G. Nord, J. Raman Spectrosc. 18 (1987) 405–407.
[26] T. Ohsaka, F. Izumi, Y. Fujiki, J. Raman Spectrosc. 7 (1978) 321–324.